

## Effect of Stacking Faults on Magnetic Flux Pinning in Boron-Doped Superconducting Diamond Films

Masanobu Shibata<sup>1,2</sup>, Taisuke Kageura<sup>1,2</sup>, Takahide Yamaguchi<sup>3</sup>,  
Yoshihiko Takano<sup>3</sup>, Hiroshi Kawarada<sup>1,2</sup>

<sup>1</sup>Waseda Univ.

3-4-1 Okubo, Shinjuku-ku, Tokyo, 169-8555, Japan

Phone: +81-3-5286-3391 E-mail: [mshibata1@ruri.waseda.jp](mailto:mshibata1@ruri.waseda.jp)

<sup>2</sup>Kagami Memorial Res. Inst. For Materials Sci. and Tech.

2-8-26, Nishiwaseda, Shinjuku-ku, Tokyo 169-0054, Japan

<sup>3</sup>National Institute for Materials Science

1-2-1 Sengen, Tsukuba-city Ibaraki, 305-0047, Japan

### Abstract

Heavily boron-doped diamond films were homoepitaxially grown on HPHT Ib (111) diamond substrates by microwave plasma assisted chemical vapor deposition. Magnetic field up to 3 T were applied to the samples to measure the magnetic field angle dependence of resistivity and observe the effect of stacking faults on magnetic flux pinning in heavily boron-doped superconducting diamonds.

### 1. Introduction

Our previous studies have shown that in heavily doped diamonds with a boron concentration of more than  $10^{21}$  cm<sup>-3</sup>, lattice strains appear and once the doped diamond film reaches a certain thickness, relaxation of the lattice strain caused by in-plane stress begins to occur. Cross-sectional transmission electron microscope (TEM) observation of heavily boron doped (111) diamond film have shown high density of planar defects such as stacking faults in boron doped diamonds with a thickness of over 500 nm [1] (Fig. 1(a)). These stacking faults could be the origin of this relaxation layer. In type II superconductors, magnetic flux pinning can occur at planar defects such as stacking faults. In this study, the magnetic field was applied to the samples from different angles to observe the flux pinning effect due to stacking faults.

### 2. Experimental

Heavily boron-doped diamond films were homoepitaxially grown on HPHT Ib (111) diamond substrates by microwave plasma (MP) CVD apparatus. The film thickness of the samples were 300 nm-1100 nm. The samples were synthesized at 800-900 °C and the chamber pressure was set to 110 Torr. Mixture gas of methane and trimethylboron with hydrogen as the carrier gas was used. The methane concentration was 5% and the B/C ratio was 18000 ppm. Resistivity of the samples were measured at temperatures from 2 K to 300 K. T<sub>c</sub> (onset) and T<sub>c</sub> (offset) were defined as the temperature at which resistivity decreases to 90% and 10% of the normal state resistivity (Fig. 2). Magnetic field of 1 T to 3 T were applied to the superconductive samples to measure the magnetic field angle dependence of resistivity.

### 3. Results and Discussion

#### 3.1 Geometrical consideration for pinning effect in stacking faults of (111) diamond substrate

The stacking faults are observed as reciprocal triangular shape in cross sectional TEM (Fig. 1(a)). The model for the structure of the stacking faults in diamond is reported to be an upside down regular tetrahedron structure [2]. The upside down tetrahedron has a vertical 3-fold axis, which passes through the bottom vertex and the center of the top face, as shown in Fig. 1(b). The calculated angle between the ridge line and the vertical axis becomes 35.3 ° and the angle between one of three inclined planes (shaded plane in Fig. 1(b)) and the vertical axis is 19.5 °. If the 3-fold axis is tilted by -22.2 ° along  $\phi=0$  line in Fig. 1(c), the shade plane become perpendicular to the horizontal plane. This geometrical position of stacking faults corresponds to the pinning condition that magnetic field is parallel to stacking fault planes.

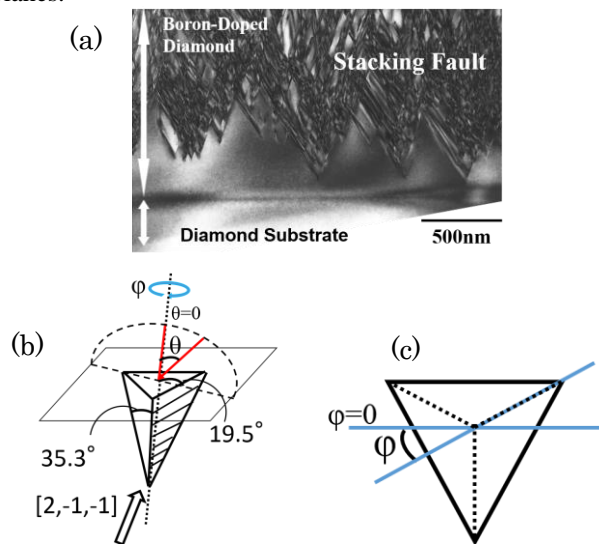


Fig. 1 (a) Cross sectional TEM, (b) bird's eye view, and (c) plan view of upside down regular tetrahedron structure of the stacking fault

#### 3.2 Magnetic field angle dependence of the superconductivity in boron-doped diamond

Two samples with a film thickness of 300 nm and 1100 nm were prepared. The 300 nm sample comprises only a strained layer and the 1100 nm sample comprises both strained and relaxed layer. The resistivity of the samples were measured at temperatures from 2 K to 300 K as shown in Fig. 2.  $T_c$  (onset) of both samples were 10.2 K and  $T_c$  (offset) of both samples were 10.0 K. The temperature at which the magnetic field will be applied to the samples was set below the  $T_c$  (offset).

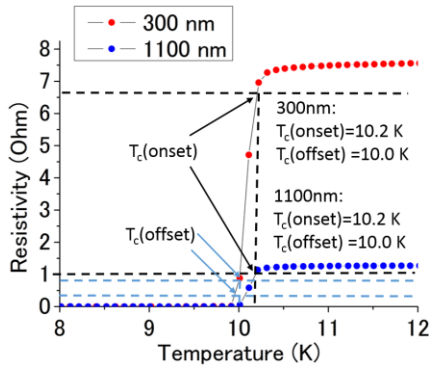


Fig. 2 Resistivity of the samples versus temperature.

Fig. 3(a), (b) shows the magnetic field angle dependence of resistivity for the 300 nm and 1100 nm sample, respectively. The temperature was set to 8 K, the range of magnetic field incident angle  $\theta$  was from  $-100^\circ$  to  $100^\circ$ , and the range of the magnetic field was set from 1 T to 3 T. In Fig. 2(a), the 300 nm sample shows that for every magnetic field strength, as the magnetic field angle increases from  $-90^\circ$  to  $0^\circ$ , the resistivity of the sample increases. In Fig. 2(b), dips, which are local minimums, in the resistivity were observed at magnetic field incident angle of  $-17^\circ$  and  $27^\circ$ . The maximum resistivity was observed at  $7^\circ$ . If there is no substrate misorientation, the maximum resistivity should appear at  $0^\circ$ , when the magnetic field is applied directly perpendicular to the substrate surface, therefore when applying the magnetic field in this particular plane, this sample shows a substrate misorientation of  $7^\circ$ . When this misorientation is considered, the angles at which the resistivity dips occur shifts to the left  $7^\circ$  and becomes  $-24^\circ$  and  $20^\circ$ , giving a close value to the calculated values. Fig. 4(a), (b) shows the magnetic field angle dependence of resistivity when the sample is rotated  $30^\circ$  and  $60^\circ$  about the vertical 3-fold  $\phi$  axis (Fig. 1(c)).

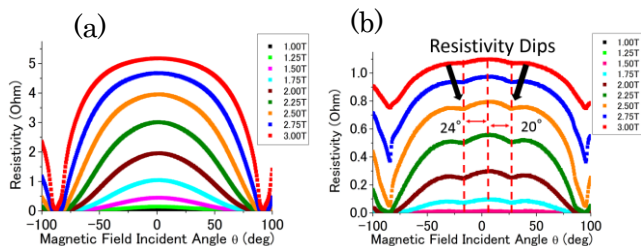


Fig. 3 Magnetic field angle dependence of resistivity of the (a) 300 nm and (b) 1100 nm sample. Tilting axis is  $[2,-1,-1]$

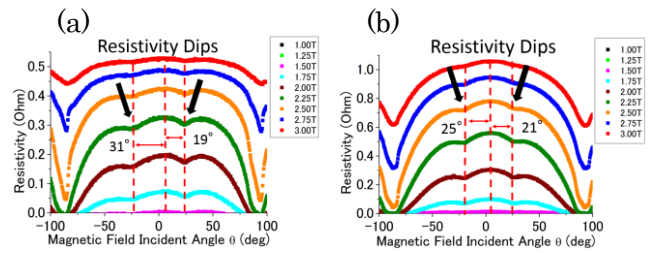


Fig. 4 Magnetic field angle dependence of resistivity of the 1100 nm sample rotated (a)  $30^\circ$ . Tilting axis is  $[1,-1,0]$  (b)  $60^\circ$ . Tilting axis  $[1,-2,1]$

In addition, as (111) diamonds are known to have a three-fold symmetry, the crystal defects are thought to have the same symmetry. In order to confirm this, the sample was rotated about the  $\phi$  axis and magnetic field was applied.

In Fig. 4(a), the dips were observed at angles of  $-26^\circ$  and  $24^\circ$ . The maximum resistivity was observed at  $5^\circ$ . In Fig. 4(b), the dips were observed at angles of  $-20^\circ$  and  $26^\circ$ . The maximum resistivity was observed at  $5^\circ$ . The angles at which resistivity dips appears for each in-plane rotation after considering the substrate misorientation is shown in Table 1.

Table 1 Resistivity Dip Angles for each In-Plane Rotation

In-Plane Rotation $\phi$ ( $^\circ$ )	Resistivity Dip 1 ( $^\circ$ )	Resistivity Dip 2 ( $^\circ$ )
0	-24	20
30	-31	19
60	-25	21

The calculated angles for pinning such as  $22.2^\circ$  and  $19.5^\circ$  in 3.1 are close to the angles at which the resistivity dips appeared. The  $22.2^\circ$  condition is obtained in the sample rotated by  $0^\circ$  and  $60^\circ$  about the  $\phi$  axis, suggesting a three-fold symmetry structure. The  $19.5^\circ$  condition corresponds to the sample rotated by  $30^\circ$ . Therefore, these resistivity dips appeared at angles where the plane defects are thought to be in the predicted model. This stacking faults could be the origin of the flux pinning effect.

#### 4. Conclusions

Magnetic field angle dependence of resistivity showed resistivity dips at two different angles. These dips are thought to be caused by magnetic flux pinning at planar defects such as stacking faults.

#### References

- [1] S. Kitagoh, H. Kawarada *et al.*, *Physica C*, **470** (2010) S610-S612.
- [2] B. E. Williams, J. T. Glass, *Journal of Materials Research* **4**, (1989) 373-384.